The AAPS Journal, Vol. 19, No. 1, January 2017 (© 2016)
DOI: 10.1208/s12248-016-9992-0

Research Article

Pharmacokinetic Modeling and Monte Carlo Simulation to Predict Interindividual Variability in Human Exposure to Oseltamivir and Its Active Metabolite, Ro 64-0802

Mototsugu Ito,[1] Hiroyuki Kusuhara,[1] Atsushi Ose,[1] Tsunenori Kondo,[2] Kazunari Tanabe,[2] Hideki Nakayama,[2] Shigeru Horita,[2] Takuya Fujita,[3] and Yuichi Sugiyama[4,5]

Received 22 May 2016; accepted 31 August 2016; published online 31 October 2016

Abstract. Oseltamivir (Tamiflu®) is a prodrug of Ro 64-0802, a selective inhibitor of influenza virus neuraminidase. There is a possible relationship between oseltamivir treatment and neuropsychiatric adverse events; although this has not been established, close monitoring is recommended on the prescription label. The objective of this study was to predict interindividual variability of human exposure to oseltamivir and its active metabolite Ro 64-0802. By leveraging mathematical models and computations, physiological parameters in virtual subjects were generated with population means and coefficient of variations collected from the literature or produced experimentally. Postulated functional changes caused by genetic mutations in four key molecules, carboxylesterase 1A1, P-glycoprotein, organic anion transporter 3, and multidrug resistance-associated protein 4, were also taken into account. One hundred thousand virtual subjects were generated per simulation, which was iterated 20 times with different random number generator seeds. Even in the most exaggerated case, the systemic areas under the concentration–time curve (AUCs) of oseltamivir and Ro 64-0802 were increased by at most threefold compared with the population mean. By contrast, the brain AUCs of oseltamivir and Ro 64-0802 were increased up to about sevenfold and 40-fold, respectively, compared with the population means. This unexpectedly high exposure to oseltamivir or Ro 64-0802, which occurs extremely rarely, might trigger adverse central nervous system effects in the clinical setting.

KEY WORDS: interindividual variability; Monte Carlo simulation; pharmacokinetics; Tamiflu®.

INTRODUCTION

Oseltamivir (Tamiflu®, Roche) is a prodrug of Ro 64-0802, a selective inhibitor of influenza virus neuraminidase, and is indicated for the treatment and prophylaxis of influenza. After a few years on the market, neuropsychiatric adverse events (NPAEs) such as abnormal behavior causing self-injury, delirium, and convulsions, some of which had fatal outcomes, were reported in a limited number of patients with influenza who were receiving Tamiflu®. This occurred mainly in pediatric/adolescent patients in Japan (1,2); in the crude NPAE reporting rates (per 1,000,000 prescriptions) in children (aged ≤16 years) and ks, respectively, were 99 and 28 events in Japan and 19 and 8 in the USA (2). Based on these findings, a precaution was added to the drug label that recommends close monitoring of patients immediately after starting treatment with Tamiflu®.

The causality between Tamiflu® treatment and NPAEs remains controversial. From the pharmacodynamic/toxicodynamic perspective, several studies have reported central nervous system (CNS) effects of oseltamivir and Ro 64-0802 in experimental animals. Yoshino *et al.* reported increased dopamine levels in the rat prefrontal cortex (3). Ono *et al.* reported oseltamivir-induced hypothermia (4), and Suzuki and Masuda demonstrated that coadministration of a dopamine receptor agonist with oseltamivir increased the number of mice exhibiting jump-down behavior (5). Usami *et al.* and Izumi *et al.* reported that both oseltamivir and Ro 64-0802 stimulate neural activities in cultured rat hippocampus slices (6,7). However, from the

Electronic supplementary material The online version of this article (doi:10.1208/s12248-016-9992-0) contains supplementary material, which is available to authorized users.

[1] Graduate School of Pharmaceutical Sciences, The University of Tokyo, Tokyo, Japan.
[2] Department of Urology, Tokyo Women's Medical University, Tokyo, Japan.
[3] College of Pharmaceutical Sciences, Ritsumeikan University, Kusatsu, Shiga, Japan.
[4] Sugiyama Laboratory, RIKEN Innovation Center, Research Cluster for Innovation, RIKEN, Kanagawa, Japan.
[5] To whom correspondence should be addressed. (e-mail: ychi.sugiyama@riken.jp)

pharmacokinetic perspective, ^{11}C-labeled oseltamivir has limited brain penetration in adult monkeys, who exhibited slightly lower brain uptake clearance compared with infant and adolescent monkeys (8). Seki *et al.* reported unchanged brain uptake of ^{11}C-labeled oseltamivir after poly I:C treatment, which simulates the immune-activation condition, in juvenile monkeys (9).

As a principle of pharmacokinetics/pharmacodynamics (toxicodynamics), the greater the drug exposure, the greater the probability of undesirable drug effects/adverse events. In addition, interindividual variability in drug exposure/responses is caused by functional differences, either randomly or nonrandomly, in drug-metabolizing enzymes, transporters, and/or target molecules. From pharmacokinetic perspectives, organ clearance is a hybrid parameter consisting of drug-related parameters (unbound fraction and intrinsic clearance) and physiological parameters (blood flow and glomerular filtration), and is one of the major determinants of interindividual variability of drug exposure. It is therefore important (1) to identify key pharmacokinetic molecules that play important roles *in vivo*, (2) to elucidate what nonrandom covariates would affect the functions of these molecules, and (3) to take into account variations in drug-related and physiological parameters.

At least four key components of intrinsic clearance have been shown to play crucial roles in oseltamivir and Ro 64-0802 pharmacokinetics *in vitro* and in animal studies: (1) hepatic metabolism of oseltamivir by carboxylesterase (CES)-1A1 to form Ro 64-0802, (2) probenecid-sensitive renal tubular secretion of Ro 64-0802 by organic anion transporters (OATs), (3) restriction of brain penetration of oseltamivir by P-glycoprotein (P-gp), and (4) restriction of brain penetration of Ro 64-0802 by OATs such as Oat3 and multidrug resistance-associated protein 4 (Mrp4) in mice (10–12). For each of these molecules, there are some genetic variants that may exhibit gain of function or reduced function, but these occur with limited frequency. Therefore, it is less likely that a sort of "worst-case" scenario of the combination of significant genetic variants identified in multiple molecules are included, identified, and analyzed in clinical trials.

The use of mathematical modeling and simulation may be helpful in investigating these issues quantitatively because they allow the incorporation of functional differences in intrinsic clearance caused by genetic mutations as a fixed effect, and outliers can be generated virtually using a combination of significant genetic variants for multiple molecules.

Kinetic parameters can be affected by interindividual variability, even within genotype groups. This means that both the population means and variances (*i.e.*, coefficient of variation, CV%) for each parameter should be taken into account to predict interindividual variability in drug exposure. This can also be incorporated into the modeling and simulation.

In this study, we used a Monte Carlo simulation approach to predict quantitatively the interindividual variability in oseltamivir and Ro 64-0802 exposure.

MATERIALS AND METHODS

Reagents

Oseltamivir phosphate and its active metabolite Ro 64-0802 were synthesized as reported previously (13). [^{3}H]*p*-Aminohippurate (PAH) (4.1 Ci/mmol), [^{3}H]estron-3-sulfate (E-sul) (43.1 Ci/mmol), and [^{14}C]tetraethylammonium (TEA) (3.2 mCi/mmol) were purchased from PerkinElmer Life and Analytical Sciences (Boston, MA). Unlabeled E-sul, PAH, and probenecid were purchased from Sigma-Aldrich (St. Louis, MO). Benzylpenicillin and cimetidine were purchased from Wako Pure Chemicals (Osaka, Japan). Anti-human OAT3 antibody was purchased from Trans Genic Inc. (Kumamoto, Japan).

Animals

All experiments using animals in this study were carried out according to the guidelines provided by the Institutional Animal Care Committee (Graduate School of Pharmaceutical Sciences, The University of Tokyo). Male FVB mice and Mdr1a/1b(−/−) mice were obtained from Taconic Farms (Germantown, NY) and maintained in Shimizu Laboratory Supplies (Kyoto, Japan). The mice were maintained under standard conditions with a reverse dark–light cycle. Food and water were available *ad libitum*. All experiments using animals in this study were carried out according to the guidelines provided by the Institutional Animal Care Committee (Graduate School of Pharmaceutical Sciences, The University of Tokyo, Tokyo, Japan).

Preparation of Human Kidney Slices and Uptake of Ro 64-0802 by Human Kidney Slices

This study protocol was approved by the ethics review boards of both the Graduate School of Pharmaceutical Sciences, The University of Tokyo (Tokyo, Japan), and Tokyo Women's Medical University (Tokyo, Japan).

All participants provided their written informed consent. Intact renal cortical tissues that had been obtained from five surgically nephrectomized patients at Tokyo Women's Medical University from November 2007 to July 2008 were used. Studies of the uptake by the human kidney slices were performed as reported previously (14). Briefly, after a 10-min incubation at 37°C in the presence of the test compound, the slices were quickly removed from the incubation buffer, washed twice in ice-cold buffer, weighed, recovered in ice-cold phosphate-buffered saline, and then homogenized using a Polytron aggregate homogenizer (Kinematica, Lucerne, Switzerland). The uptake activities of OAT1, OAT3, and organic cation transporter 2 (OCT2) in the human kidney slices were measured in every experiment using 0.1 μM tracer or 1.0 mM excess PAH, E-sul, and TEA as reference compounds for OAT1, OAT3, and OCT2, respectively.

Construction of OAT3 Variant cDNA

The full-length human OAT3 constructs used in this study were subcloned into the pIRES2–EGFP vector as reported previously (15). Each of the two nonsynonymous OAT3 variants (I175V and A389V) identified in previous reports (16) was then constructed by site-directed mutagenesis of the OAT3 reference-containing plasmid using the QuickChange mutagenesis protocol (Stratagene, La Jolla, CA). The sequence of each variant was confirmed by complete DNA sequencing to ensure that the appropriate

nucleotide change had occurred and to confirm that no other alterations had been introduced. The primer sequences were I175V: forward primer, 5′-CACCTTCCCCGTCTACATGG-3′, and reverse primer, 5′-CCATGTAGACGGGG AAGGTG-3′, and A389V: forward primer, 5′-CAGG CCGCTGTCCTGCTCCTG-3′, and reverse primer, 5′-CAGGAGCAGGACGGCGGCCTG-3′.

Expression of OAT3 Variants in Mammalian Cells and Transport Studies in OAT3-Transfected Human Embryonic Kidney (HEK) 293 Cells

Each of the two nonsynonymous OAT3 variants (I175V and A389V) was constructed by site-directed mutagenesis of the wild-type OAT3 cDNA-containing plasmid using the QuickChange mutagenesis protocol (Stratagene, La Jolla, CA). DNA sequences of each variant were confirmed using an automated DNA sequencer (ABI PRISM 3100; Applied Biosystems, Foster City, CA). Wild-type OAT3 and its variant-overexpressing HEK293 cell lines were constructed using Lipofectamine 2000 (Invitrogen) according to the manufacturer's protocol, and stably transfected cells were selected by G418 (0.8 mg/mL) (Invitrogen) in the culture medium. HEK 293 cells transfected with empty vector (mock cells) served as a negative control. The transport study was performed as described previously (17). The uptake of each ligand by OAT3-overexpressing transfectants was subtracted from that of mock cells to obtain the OAT3-mediated uptake clearance. The cell surface expression level of OAT3 was quantified using a cell surface biotinylation method followed by Western blot analysis, as described previously (18), and was used for the calculation of the uptake properties of each OAT3 variant.

Determination of Brain-to-Plasma Concentration Ratio of Oseltamivir and Ro 64-0802 Following Subcutaneous Infusion of Oseltamivir

Male FVB mice and Mdr1a/1b(−/−) mice (10–18 weeks of age) weighing 25–30 g were used for these experiments. An Alzet® osmotic pump (Cupertino, CA, 8 μL/h) was implanted into mice under the skin on the back under pentobarbital anesthesia (51.8 mg/kg). The mice received a continuous subcutaneous infusion of oseltamivir at 400 nmol/h. Blood samples were collected from the postcaval vein from mice under pentobarbital anesthesia at 24 h after the dose, and the brain was excised immediately. Plasma was obtained by centrifugation of the blood samples (10,000*g*). The esterase inhibitor dichlorvos (200 μg/mL) was used to prevent *ex vivo* hydrolysis of oseltamivir to Ro 64-0802 in the blood and plasma (19,20). The plasma and brain concentrations of Ro 64-0802 were determined using liquid chromatography–mass spectrometry analysis (10,11).

Parameter Estimation of the Clinical Pharmacokinetics of Oseltamivir and Ro 64-0802

The plasma concentration–time profiles of oseltamivir and Ro 64-0802 in humans after a single oral administration of oseltamivir (150 mg qd) were obtained from a previous report (21) using DataThief III software (available at http://datathief.org/). Although the dose of 150 mg qd is not the same as a clinical dose of 75 mg bid, obtaining key pharmacokinetic parameters using this method is still considered to be valid because of the dose-proportional pharmacokinetics of each of oseltamivir and Ro 64-0802 (application form: http://www.info.pmda.go.jp/go/interview/1/450045_6250021M1027_1_027_1F). The reported values (application form) for unbound plasma protein binding fraction and erythrocyte partitioning ratio of oseltamivir and Ro 64-0802 were used. Assuming a hematocrit level of 0.45, R_b values were calculated as shown in Table I. Considering the reported pharmacokinetic properties of oseltamivir, we assumed that oseltamivir is readily absorbed from the gastrointestinal tract ($F_a \cdot F_g = 1$) and extensively metabolized in the liver (the rest is eliminated by hepatic metabolism and urinary excretion). We also assumed that Ro 64-0802 is synthesized mainly in the liver and is excreted into urine but not into bile, and constructed the following equations.

$$\frac{dC_{\text{blood, oseltamivir}}}{dt} = \frac{k_a \times \text{dose} \times \left(1 - \frac{CL_{H,\text{oseltamivir}}}{Q_H}\right)}{V_{d,\text{oseltamivir}}} - \frac{\left(CL_{H,\text{oseltamivir}} + CL_{R,\text{oseltamivir}}\right)}{V_{d,\text{oseltamivir}}} \times C_{\text{blood, oseltamivir}} \quad (1)$$

Table I. Summary of Pharmacokinetic Parameters for Oseltamivir and Ro 64-0802

	Population mean	CV%
Q_h	1.70 (L/min)[a]	19.5[a]
Q_r	1.23 (L/min)[b]	8.30[b]
E_h	0.735[c, d]	–
F_h	0.265[c, d]	–
$f_{b\_oseltamivir}$	0.460[e]	5.80[i]
$f_{b\_Ro\ 64\text{-}0802}$	1.53[e]	5.80[i]
$R_{b\_oseltamivir}$[k]	1.27	–
$R_{b\_Ro\ 64\text{-}0802}$[k]	0.640	–
GFR	125 (mL/min)[f]	20.0[j]
$CL_{r\_plasma\_oseltamivir}$	28.9 (L/h)[g]	–
$CL_{r\_blood\_oseltamivir}$	379.5 (mL/min)	20.0[j]
$CL_{r\_plasma\_Ro\ 64\text{-}0802}$	20.0 (L/h)[g]	–
$CL_{sec\_blood\_Ro\ 64\text{-}0802}$	330 (mL/min)[h]	–
$CL_{int\_renal\_Ro\ 64\text{-}0802}$	305 (mL/min)	20.0[j]
$CL_{int\_liver\_oseltamivir}$	12.0 (L/min)	20.0[j]

[a] (22)
[b] (23)
[c] Obtained by in-house analysis (fitted using Multi (Runge))
[d] Calculated assuming that $F_a \cdot F_g = 1$
[e] Application form
[f] (25)
[g] (21)
[h] Calculated assuming that Ro 64-0802 is not reabsorbed
[i] (24)
[j] Assumed
[k] $R_b = (1 - \text{Ht})/(\text{erythrocyte partitioning ratio})$

$$\frac{dC_{\text{blood,Ro 64-0802}}}{dt} = \frac{k'_{\text{eff}} \times V_{\text{h}}}{V_{\text{d,Ro 64-0802}}} \times C_{\text{liver, Ro 64-0802}} - \frac{\left(\text{CL}_{\text{R,Ro 64-0802}}\right)}{V_{\text{d,Ro 64-0802}}} \times C_{\text{blood, Ro 64-0802}} \quad (2)$$

$$\frac{dX_{\text{liver, Ro 64-0802}}}{dt} = \text{CL}_{\text{H,oseltamivir}} \times C_{\text{blood,oseltamivir}} - k'_{\text{eff}} \times X_{\text{liver, Ro 64-0802}} \quad (3)$$

Equations 1–3 represent the differential equations for the blood concentrations of oseltamivir and Ro 64-0802, and hepatic content of Ro 64-0802, respectively. C, k_{a}, CL_{H}, CL_{R}, Q_{h}, k'_{eff}, V_{h}, and V_{d} represent the drug concentration, absorption rate constant, hepatic clearance, renal clearance, hepatic blood flow rate, elimination rate constant for the hepatic sinusoidal efflux of Ro 64-0802, liver volume, and distribution volume, respectively. Initial conditions are as follows;

$$\text{Eq. 1} : C_{\text{blood,oseltamivir}} = 0$$

$$\text{Eq. 2} : C_{\text{blood,Ro 64-0802}} = 0$$

$$\text{Eq. 3} : X_{\text{liver,Ro 64-0802}} = \text{dose} \times \frac{\text{CL}_{\text{H,oseltamivir}}}{Q_{\text{H}}}$$

Unknown parameters such as k_{a}, k'_{eff}, V_{d}, and CL_{H} were obtained using an iterative nonlinear least-square method using the Multi (Runge) program (available at http://www.pharm.kyoto-u.ac.jp/byoyaku/Kinetics/download.html).

$\text{CL}_{\text{H,oseltamivir}}/Q_{\text{H}} \times \text{dose}$ was regarded as the initial amount (X) of Ro 64-0802 in the liver.

Mathematical Models for Peripheral and Central Exposures to Oseltamivir and Ro 64-0802

The areas under the blood concentration–time curve ($\text{AUC}_{\text{blood}}$) of oseltamivir and Ro 64-0802 after a single oral administration of oseltamivir are represented as follows:

$$\text{AUC}_{\text{blood,oseltamivir}} = \frac{F_{\text{H}} \times \text{dose}}{\text{CL}_{\text{tot,oseltamivir}}} = \frac{\left(1 - \frac{\text{CL}_{\text{H,oseltamivir}}}{Q_{\text{H}}}\right) \times \text{dose}}{\text{CL}_{\text{H,oseltamivir}} + \text{CL}_{\text{R,oseltamivir}}} \quad (4)$$

$$\text{AUC}_{\text{blood,Ro 64-0802}} = \frac{\left(\frac{\text{CL}_{\text{H,oseltamivir}}}{Q_{\text{H}}} \times \text{dose}\right) + \left(\text{AUC}_{\text{blood,oseltamivir}} \times \text{CL}_{\text{H,oseltamivir}}\right)}{\text{CL}_{\text{R,Ro 64-0802}}}, \quad (5)$$

where F_{H} and CL_{tot} represent hepatic availability and total clearance, respectively. Assuming a well-stirred model, $\text{CL}_{\text{H, oseltamivir}}$ and $\text{CL}_{\text{R, Ro 64-0802}}$ were computed using randomly generated simulated blood unbound fractions, blood flow rates, and intrinsic clearances. The functional changes in CES1A1 caused by genetic variants were equal to the changes in the hepatic intrinsic clearance of oseltamivir. In addition, because the present study found that OAT3 but not OAT1 plays crucial roles in the renal tubular secretion of Ro 64-0802, the functional changes in OAT3 caused by genetic variants were equal to the changes in renal intrinsic clearance of Ro 64-0802.

The areas under the brain concentration–time curve ($\text{AUC}_{\text{brain}}$) of oseltamivir and Ro 64-0802 are represented as follows (a schematic diagram is shown in Fig. 1):

$$V_{\text{brain,oseltamivir}} \times \frac{dC_{\text{brain,oseltamivir}}}{dt} = f_{\text{B,oseltamivir}} \times C_{\text{blood,oseltamivir}} \times \text{PS}_{\text{inf,oseltamivir}} - f_{\text{brain,oseltamivir}} \times C_{\text{brain,oseltamivir}} \times \left(\text{PS}_{\text{eff,oseltamivir}} + \text{CL}_{\text{met,oseltamivir,brain}}\right) \quad (6)$$

$$V_{\text{brain,Ro 64-0802}} \times \frac{dC_{\text{brain,Ro 64-0802}}}{dt} = f_{\text{B,Ro 64-0802}} \times C_{\text{blood,Ro 64-0802}} \times \text{PS}_{\text{inf,Ro 64-0802}} - f_{\text{brain,Ro 64-0802}} \times C_{\text{brain,Ro 64-0802}} \times \text{PS}_{\text{eff,Ro 64-0802}} + f_{\text{brain,oseltamivir}} \times C_{\text{brain,oseltamivir}} \times \text{CL}_{\text{met,oseltamivir,brain}}, \quad (7)$$

where f_{B}, f_{brain}, PS_{inf}, PS_{eff}, and CL_{met} represent the unbound fraction in the blood, unbound fraction in the brain, brain uptake clearance, brain efflux clearance, and brain metabolic clearance, respectively. Initial conditions are as follows:

$$\text{Eq. 6} : C_{\text{brain,oseltamivir}} = 0$$

$$\text{Eq. 7} : C_{\text{brain,Ro 64-0802}} = 0$$

To determine the AUC, we integrated the time in the above equations from 0 to infinity as follows:

$$\text{AUC}_{\text{brain,oseltamivir}} = \text{AUC}_{\text{blood,oseltamivir}} \times \frac{f_{\text{B,oseltamivir}}}{f_{\text{brain,oseltamivir}}} \times \frac{\text{PS}_{\text{inf,oseltamivir}}}{\left(\text{CL}_{\text{met,oseltamivir,brain}} + \text{PS}_{\text{eff,oseltamivir}}\right)} \quad (8)$$

$$\text{AUC}_{\text{brain,Ro 64-0802}} = \frac{\text{AUC}_{\text{blood,Ro 64-0802}} \times f_{\text{B,Ro 64-0802}} \times \text{PS}_{\text{inf,Ro 64-0802}} + \text{AUC}_{\text{brain,oseltamivir}} \times f_{\text{brain,oselatamivir}} \times \text{CL}_{\text{met,oseltamivir,brain}}}{f_{\text{brain,Ro 64-0802}} \times \text{PS}_{\text{eff,Ro 64-0802}}}. \quad (9)$$

Monte Carlo Simulation

Monte Carlo simulation was conducted according to the methods prescribed by Kato *et al.* (26). We first prepared several sets of 100,000 pseudorandom numbers between 0 and 1, followed by the assignation of the genotype of each transporter and metabolic enzyme based on the allele frequencies of each genetic mutant. For example, for a mutant whose allele frequency is 0.01, the patient would be a carrier of this mutant if he/she received a pseudorandom number from 0 to 0.01. By repeating this procedure twice, we determine the diplotype of one gene in each patient. As shown in Table I, using the mean and CV% values (a log-normal distribution was assumed with no covariance), we generated 100,000 virtual subjects with a variety of blood flow rates, protein binding ratios, glomerular filtration rates, and intrinsic clearances. The number of virtual subjects per simulation was 100,000, and the simulation was repeated 20 times to obtain summary statistics. Simulations were computed using R (version 3.0.0).

Effects of Genetic Mutations on Protein Function

The effects of each genetic mutation on the transport and metabolic activities of the molecules are summarized in Table II. As for the brain exposure to oseltamivir and Ro 64-0802, some extreme cases were chosen to solve the mathematical equations (Eqs. 8 and 9) more simply and easily because influx, metabolic, and efflux clearances could not be determined quantitatively in humans. This was done under the assumptions that (1) the efflux clearance of oseltamivir is much higher than the metabolic clearance of oseltamivir in the brain (efflux >> metabolism), (2) the efflux clearance of oseltamivir is equal to the metabolic clearance of oseltamivir in the brain (efflux = metabolism), (3) the efflux clearance of oseltamivir is much lower than the metabolic clearance of oseltamivir in the brain (efflux << metabolism), and (4) the brain uptake of Ro 64-0802 is much larger than the brain metabolism (synthesis << brain uptake, Ro 64-0802 only).

Based on the schematic diagram shown in Fig. 1, the roles of transporters in the brain distribution of oseltamivir and Ro 64-0802 were calculated. The $K_{p,brain}$ of oseltamivir at steady state was defined as follows:

$$K_{p,\,brain} = \frac{C_{brain}}{C_{plasma}} \tag{10}$$

$$f_p \times C_p \times PS_{inf,oseltaivir,brain} = f_{brain} \times C_{brain} \times PS_{eff,oseltaivir,brain}, \tag{11}$$

where PS_{inf}, PS_{eff}, and f_{brain} represent the uptake, efflux, and unbound fraction of oseltamivir in the brain, respectively. We assumed that MDR1 plays a predominant role in oseltamivir efflux and that no uptake transporter is involved in oseltamivir influx. Based on this assumption, Eq. 10 can be represented as:

$$K_{p,\,brain} = \frac{C_{brain}}{C_{plasma}} = \frac{f_p \times PS_{inf,oseltamivir}}{f_{brain} \times PS_{eff,oseltamivir}} = \frac{f_p \times PS_{dif,oseltamivir}}{f_{brain} \times \left(PS_{dif,oseltamivir} + PS_{MDR1,oseltamivir}\right)}. \tag{12}$$

Because the present study showed that the $K_{p,brain}$ was 19.9-fold higher in Mdr1a/1b(−/−) mice than in wild-type mice, as per Eq. 12, P-gp-mediated efflux clearance ($PS_{MDR1,oseltamivir}$) was regarded as being 18.9-fold higher than the clearance for passive diffusion ($PS_{dif,oseltamivir}$). In human brain capillary endothelial cells, CES1A1 expression has been detected by immunohistochemical staining (35). The effect of genetic mutation of CES1A1 on the metabolic clearance of oseltamivir in the brain was assumed to be the same as that in the liver (*i.e.*, CES1A1 is considered to play an exclusive role in brain metabolism of oseltamivir). Taking these factors into consideration, the relative functional changes in P-gp and CES1A1 attributed to genetic variants compared with the wild-type were used to solve Eq. 8 to obtain the fold-increase values for the brain AUC.

When investigating the brain distribution of Ro 64-0802, we considered that OAT3 and MRP4 are responsible for the efflux of Ro 64-0802 at the abluminal and luminal membranes, respectively, in the blood–brain barrier (BBB). Influx and efflux clearance of Ro 64-0802 is represented as follows:

$$CL_{inf,\,Ro\,64\text{-}0802} = \left(PS_{dif,Ro\,64\text{-}0802}\right) \times \frac{PS_{dif,Ro\,64\text{-}0802}}{2 \times PS_{dif,Ro\,64\text{-}0802} + PS_{MRP4,Ro\,64\text{-}0802}} \tag{13}$$

$$CL_{eff,\,Ro\,64\text{-}0802} = \left(PS_{dif,Ro\,64\text{-}0802} + PS_{OAT3,Ro\,64\text{-}0802}\right) \times \frac{PS_{dif,Ro\,64\text{-}0802} + PS_{MRP4,Ro\,64\text{-}0802}}{2 \times PS_{dif,R\,o64\text{-}0802} + PS_{MRP4,Ro\,64\text{-}0802}}, \tag{14}$$

where CL_{inf}, CL_{eff}, PS_{dif}, PS_{OAT3}, and PS_{MRP4} represent intrinsic clearance, efflux clearance, clearance of passive diffusion, and OAT3- and MRP4-mediated efflux clearance of Ro 64-0802, respectively. Ose *et al.* (2008a) studied wild-type, Oat3(−/−), and Mrp4(−/−) mice and reported that Oat3 and Mrp4 are important to the efflux of Ro 64-0802 across the BBB. In Oat3(−/−) mice, which can be regarded as having abolished Oat3 function, the elimination rate constant of Ro 64-0802 decreased from 0.0127 (/min) to 0.00317 (/min), and we assumed the functional change in Oat3 caused by genetic mutation directly affects the brain efflux clearance of Ro 64-0802 (10). By contrast, $PS_{dif,Ro\ 64\text{-}0802}$ and $PS_{MRP4,Ro\ 64\text{-}0802}$ could not be obtained directly; $PS_{dif,Ro\ 64\text{-}0802}$ was assumed to

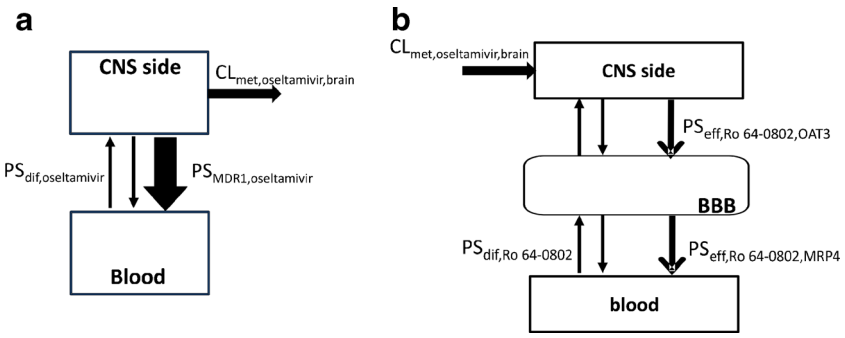

Fig. 1. Schematic diagrams of the model for the brain distribution of oseltamivir (**a**) and Ro 64-0802 (**b**). The compartment model to describe the exchange of oseltamivir (**a**) and Ro 64-0802 (**b**) between the blood and CNS side was shown across the BBB where active transports mediated by P-gp and OAT3 and MRP4 at the BBB as well as passive diffusion were taken into consideration for oseltamivir and Ro 64-0802, respectively. $PS_{inf,Ro\ 64\text{-}0802}$ and $PS_{eff,Ro\ 64\text{-}0802}$ that were used in Eqs. 13 and 14 were obtained assuming rapid equilibrium in the BBB compartment

be negligibly small compared with $PS_{MRP4,Ro\ 64\text{-}0802}$. The relative functional changes in OAT3 and MRP4 caused by genetic mutation were incorporated into the model, and Eqs. 13 and 14 were solved to obtain the brain AUC of Ro 64-0802.

Statistical Analyses

Student's *t* test and one-way ANOVA followed by Dunnett's test were used to identify significant differences between groups when appropriate. Significance was set at $p < 0.05$.

RESULTS

Uptake of Ro 64-0802 by Human Kidney Slices and OAT1- and OAT3-Overexpressing HEK293 Cells

Uptake of Ro 64-0802 (10 μM) by human kidney slices was linear up to 10 min and was significantly inhibited by

Table II. Summary of Genetic Mutations in OAT3, CES1A1, MRP4, and MDR1

Gene	Amino acid change	CDS position	Genotype	Allele/genotype/diplotype frequency	Activity (%)
OAT3	R149S[a]			0.004	0
	Q239stop[a]			0.002	0
	I260R[a]			0.002	0
	R277W[a]			0.002	50.0[a]
	I305P[a]			0.009	50.0[a]
	I175V[b]			0.05	13.6[l]
	A389V[c]			0.008	9.50[l]
CES1A1	R182H[d]		G/A	0.024[f]	70.0[d]
		(−816A)[e]	A/C	0.286[e]	125[e]
			C/C	0.105[e]	150[e]
MRP4[g]	E757K			0.204	20.0
MDR1[h,i,j]			C-G-T	0.162[k]	11.3
			C-T/A-C	0.145[k]	56.2
			C-T/A-T	0.064[k]	55.1[m]
			T-G-T	0.082[k]	14.3
			T-T/A-T	0.304[k]	53.6
(C3435T-G2677T/A-C1236T)					

[a] (27)
[b] (28)
[c] (16)
[d] (12)
[e] (29)
[f] NCBI rs2307243
[g] (30)
[h] (31)
[i] (32)
[j] (33)
[k] (34)
[l] In-house data (supplemental Fig. 3A and B)
[m] Activity (%) of MDR1 haplotype for 3435C-2677A-1236T protein was assumed to be 100%

1 mM PAH, benzylpenicillin, probenecid, or cimetidine (63.5% ± 4.62%, 59.1% ± 4.97%, 50.8% ± 3.34%, and 67.1% ± 4.25% of control values, respectively, $p < 0.05$), but not by 1 mM TEA (108% ± 9%) (Supplemental Fig. 1A). A significant inhibitory effect of probenecid on the uptake was observed at 10 μM and higher (Supplemental Fig. 1B), whereas inhibition by cimetidine was observed only at 1 mM (Supplemental Fig. 1C).

The time-dependent uptake of Ro 64-0802 in OAT3-overexpressing HEK293 cells was linear up to 10 min (Supplemental Fig. 2B). The OAT3-mediated uptake clearance of Ro 64-0802, defined by subtracting from the uptake in vector transfectants, was 1.29 μL/min/mg protein. OAT1-specific uptake of Ro 64-0802 of OAT1 was rarely observed (Supplemental Fig. 2A).

Characterization of the Nonsynonymous Mutants of OAT3 (I175V) and (A389V)

The uptake of [^{3}H]E-sul (0.1 μM) and Ro 64-0802 (5.0 μM) by the empty vector, wild-type, and I175V and A389V OAT3-overexpressing HEK293 cells was measured. The uptake of [^{3}H]E-sul and Ro 64-0802 was compared between the empty vector-transfected cells and each type of OAT3-overexpressing cell line (Supplemental Fig. 3A). The cell surface expression of each OAT3 variant and wild-type OAT3 was quantified by Western blot analysis followed by band density quantification (Supplemental Fig. 3B). Both I175V and A389V variants were reduced function variants when the activity of the unit transporter molecule was compared. The uptake values for E-sul by cell surface I175V and A389V variants were 13.7% ± 1.03% and 12.0% ± 0.18%, respectively, compared with wild-type OAT3. The respective uptake values for Ro 64-0802 were 13.6% ± 1.27% and 9.5% ± 0.09%.

Limited Penetration of Oseltamivir into the Brain Across the BBB by P-gp

To characterize the P-gp-mediated efflux at the BBB, oseltamivir was given by subcutaneous infusion for 24 h, and the brain-to-plasma concentration ($K_{p,brain}$) of oseltamivir was determined. The $K_{p,brain}$ of oseltamivir was 19.9-fold higher in Mdr1a/1b(−/−) mice than in wild-type mice (1.27 ± 0.263 *vs* 0.064 ± 0.008), whereas the $K_{p,brain}$ of Ro 64-0802 did not differ significantly between Mdr1a/1b(−/−) mice and wild-type mice (Supplemental Fig. 4).

A Model to Fit the Blood Concentration–Time Profile of Oseltamivir and Ro 64-0802

A model of first-order absorption with a one-compartment disposition pharmacokinetic was built. The pharmacokinetic parameters of oseltamivir and Ro 64-0802 were obtained based on data reported from phase 1 clinical studies (21,36) and tested using a nonlinear least-square method using the Multi (Runge) program. Simulated systemic concentration–time curves for oseltamivir and Ro 64-0802 described the actual observed data well (Fig. 2). The obtained extraction ratio in the liver (Eh) was 0.735, assuming an $F_a \cdot F_g$ of 1.

Prediction of Systemic Exposure to Oseltamivir and Ro 64-0802

One hundred thousand virtual subjects were generated, and the interindividual variabilities of systemic AUCs for oseltamivir (Fig. 3) and Ro 64-0802 (Fig. 4) were computed and analyzed using R. Those subjects carrying varying genotypes for CES1A1 and OAT3, and their physiological and pharmacokinetic parameters (*e.g.*, blood flow rates, unbound fractions), were varied within the designated population means (functional changes caused by single nucleotide polymorphisms (SNPs) were also taken into account as fixed effects) and CV% under a log-normal distribution (shown in Tables I and II). The median values of population mean (%CV) out of 20 simulations for plasma AUC of oseltamivir and Ro 64-0802 were 306 μg·h/L (25.3%) and 6777 μg·h/L (15.5%), respectively, which were comparable to the data reported previously (253 μg·h/L (24.5%) and 5436–6218 μg·h/L (12.2–23.8%)) (21). In our simulation, even in the most exaggerated case, the systemic AUCs of oseltamivir and Ro 64-0802 were increased by up to threefold compared with the population means (Figs. 3 and 4; shown in inset). The predicted population means and variabilities of systemic AUCs for oseltamivir and Ro 64-0802 were similar to those for the reported data (21,36).

Prediction of Brain Exposure to Oseltamivir and Ro 64-0802

Figure 1 shows schematic diagrams of the molecular mechanisms responsible for the brain distribution of oseltamivir (Fig. 1a) and Ro 64-0802 (Fig. 1b). The mathematical models incorporated passive diffusion and transporter-mediated membrane transport (MDR1 and OAT3/MRP4 for brain efflux of oseltamivir and Ro 64-0802, respectively). None of the permeability surface area products (PS) and metabolic clearances in the human brain could be obtained directly, and thus, some extreme cases were chosen to solve the mathematical equations more simply and easily. This was done by using (1) the relative fold changes in subjects with genetic variants compared with wild type to

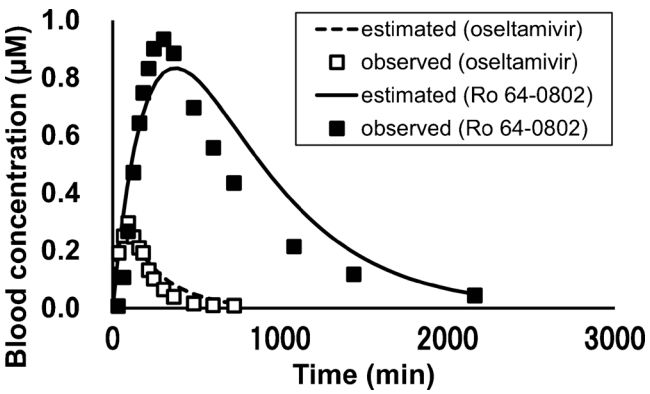

Fig. 2. Mathematical fitting of blood concentration–time profiles of oseltamivir and Ro 64-0802 after a single oral administration of oseltamivir (150 mg). The blood concentration–time profiles of oseltamivir (*dotted line*) and Ro 64-0802 (*solid line*) were fitted using the Multi (Runge) program. *Open and closed squares* represent the observed blood concentrations of oseltamivir and Ro 64-0802, respectively

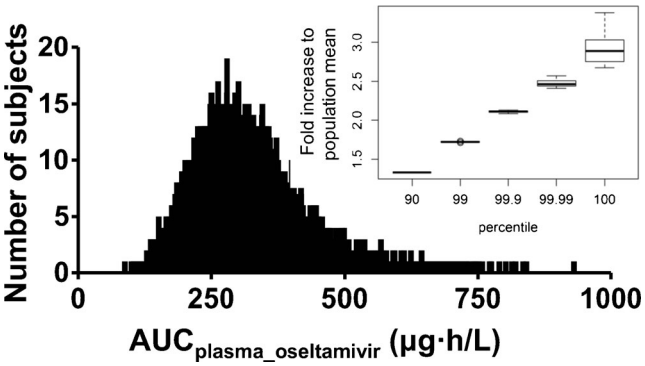

Fig. 3. Distribution of predicted plasma AUC for oseltamivir in 100,000 virtual subjects after a single oral administration of oseltamivir (150 mg). The histogram shows representative results of one of 20 simulations. The *inset figure* represents a box plot of the 90th, 99th, 99.9th, 99.99th, and 100th percentiles of fold increases relative to the population mean and summarized from 20 simulations

incorporate the influence of genetic mutations and (2) the assumption that the brain pharmacokinetics of oseltamivir is identical in mice and humans. The brain AUCs of oseltamivir and Ro 64-0802 were increased by up to sevenfold (Fig. 5) and 40-fold (Fig. 6), respectively, compared with the population mean values, which contained a variety of combinations of the variants.

Sensitivity Analysis

The influence of the functional changes in CES1, OAT3, P-gp, and MRP4 caused by genetic variants in the systemic and brain AUCs of oseltamivir and Ro 64-0802 was evaluated by sensitivity analysis (Fig. 7). Variations from 10-fold reductions up to 10-fold increases in each molecule were assumed and compared with those of the wild type. The blood AUC of oseltamivir was more sensitive to functional changes in CES1A1, whereas the blood AUC of Ro 64-0802 was more sensitive to functional changes in OAT3 and was hardly affected by changes in CES1A1. The brain AUCs of oseltamivir and Ro 64-0802 were dependent on the model assumptions.

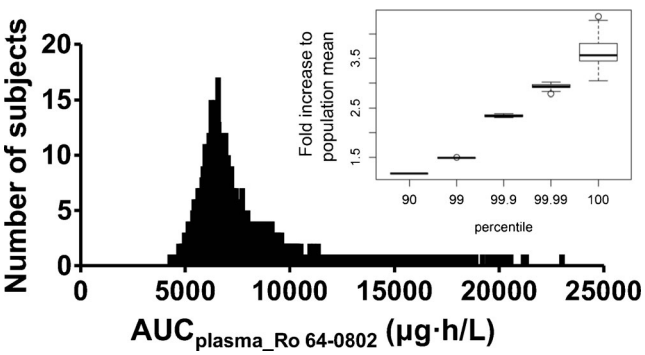

Fig. 4. Distribution of predicted plasma AUC of Ro 64-0802 in 100,000 virtual subjects after single oral administration of oseltamivir (150 mg). The histogram shows a representative figure of one of 20 simulations. The *inset figure* represents a box plot of the 90th, 99th, 99.9th, 99.99th, and 100th percentiles of fold increases relative to the population mean and summarized from 20 simulations

DISCUSSION

The clinical relevance of the abnormal behavior thought to be caused by taking oseltamivir has not been clarified. In this study, we hypothesized that the combination of the genetic mutations associated with significant functional changes would alter the pharmacokinetics of oseltamivir and/or Ro 64-0802, which might produce the unexpected incidents with rare frequency. Using a Monte Carlo approach, we virtually predicted and depicted the distribution of systemic and brain exposures (AUCs) for oseltamivir and Ro 64-0802 by taking into account the interindividual variability of each pharmacokinetic parameter such as blood flow rate, unbound protein binding fraction, and the effects of genetic mutations on intrinsic clearance.

We conducted some *in vitro* and *in vivo* experiments to obtain an insight into the pharmacokinetics of oseltamivir and Ro 64-0802. First, the mechanism responsible for the renal tubular secretion of Ro 64-0802, the major elimination pathway from the systemic circulation, was characterized *in vitro*. We have previously demonstrated that the uptake in human kidney slices correlates linearly with the renal clearance of the corresponding compounds (37). The results of the uptake study with human kidney slices suggested that OATs, but not organic cation transporters, are responsible for renal uptake of Ro 64-0802. Hill *et al.* reported the involvement of OAT1 by demonstrating significant uptake of Ro 64-0802 in OAT1-overexpressing cell lines (36). However, in the present study, OAT1 hardly recognized Ro 64-0802 as a substrate, but OAT3 did. Hill *et al.* denied the possibility of OAT3 involvement, as shown by the finding of no significant clinical drug–drug interaction with cimetidine, an OAT3 substrate. However, at the concentration relevant to the maximum unbound plasma concentration of cimetidine at a dose of 400 mg (5.2 μM) (38), the inhibitory effect of cimetidine (1–100 μM) on Ro 64-0802 uptake by human kidney slices was not observed. This indicates that the absence of a clinical drug interaction with cimetidine on the renal uptake of Ro 64-0802 may not exclude the contribution of OAT3. In addition, we found that two nonsynonymous variants of OAT3 (I175V and A389V) are variants with significantly reduced function *in vitro*.

Second, the $K_{p,brain}$ of oseltamivir in Mdr1a/1b(−/−) mice was determined after a longer duration than in the previous report (120 min) (11). The $K_{p,brain}$ of oseltamivir was about threefold higher at 24 h than at 2 h. All of the information was included in the subsequent model analysis.

Using 100,000 virtual subjects with a series of pharmacokinetic parameters, we computed the individual blood and brain AUCs of oseltamivir and Ro 64-0802. Because of the nature of our interest in the maximum fold increase in AUC in the most extreme case within the virtual population, the values were susceptible to random seeding. We therefore repeated the simulations 20 times and took the median values to bolster the prediction probability. The maximum brain AUCs of oseltamivir and Ro 64-0802 were about sevenfold and 40-fold higher, respectively, compared with the population mean, which included a variety of combinations of the variants. The EC_{50} of oseltamivir and Ro 64-0802 against the abnormal population synchronized burst in cultured rat hippocampus slices were 10.2 and 0.7 μM, respectively (7),

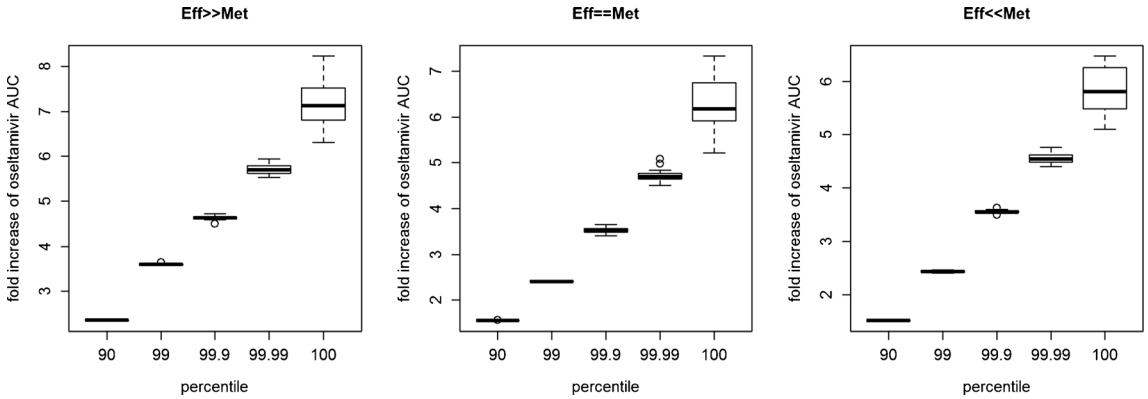

Fig. 5. Summary of the brain AUC of oseltamivir after a single oral administration of oseltamivir (150 mg). The figures represent box plots of the 90th, 99th, 99.9th, 99.99th, and 100th percentiles of fold increases relative to the population mean and summarized from 20 simulations under the assumptions that the efflux clearance of oseltamivir is much higher than the metabolic clearance of oseltamivir in the brain (*left*), equal to the metabolic clearance of oseltamivir in the brain (*middle*), and much less than the metabolic clearance of oseltamivir in the brain (*right*)

which are greater than their concentrations in the cerebrospinal fluid (CSF) (7.7 and 67.8 nM, for oseltamivir and Ro 64-0802, respectively (39)) after a single oral administration of oseltamivir (150 mg) in humans. The clinical dose of oseltamivir is 75 mg twice daily for adults and even less for children. However, assuming the most extreme cases, the CSF concentration of Ro 64-0802 could exceed the EC_{50} and may trigger NPAEs of oseltamivir.

The effects of functional changes in CES1A1, OAT3, MRP4, and MDR1 on the blood and brain AUCs of oseltamivir and Ro 64-0802 were calculated further by sensitivity analysis. As expected, sensitivity analysis revealed that the brain AUC of oseltamivir is highly sensitive to the CES1A1 function in all scenarios (Fig. 7c–e) and to MDR1 in some cases when the brain efflux of oseltamivir could not be ignored. In particular, because the functional changes in

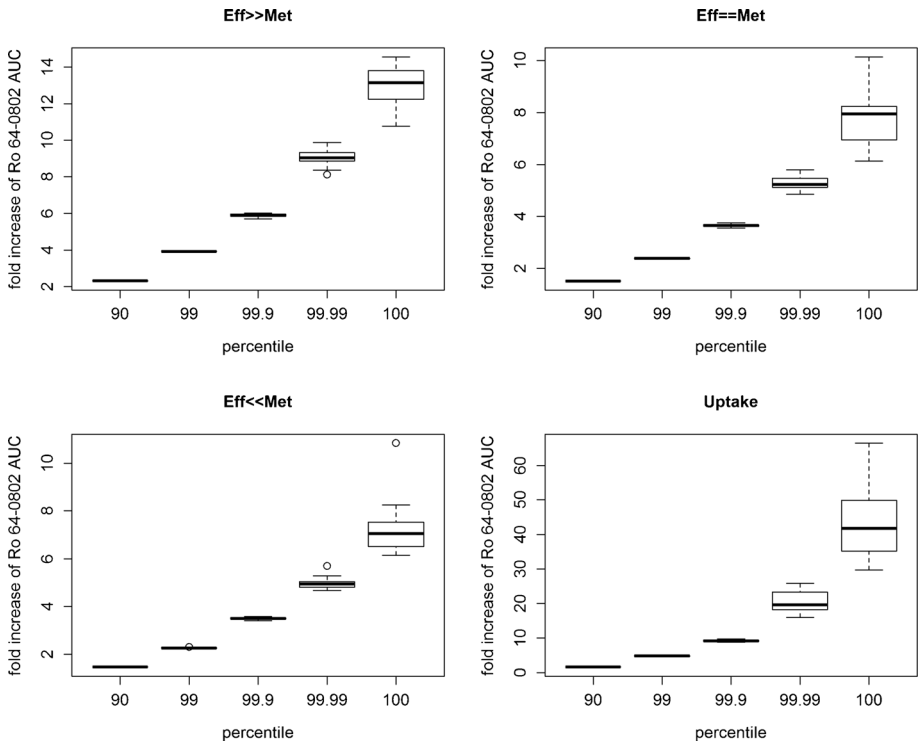

Fig. 6. Summary of the brain AUC for Ro 64-0802 after a single oral administration of oseltamivir (150 mg). The figures represent box plots of the 90th, 99th, 99.9th, 99.99th, and 100th percentiles of fold increases relative to the population mean and summarized from 20 simulations under the assumptions that the efflux clearance of oseltamivir is much higher than the metabolic clearance of oseltamivir in the brain (*top left*), the efflux clearance of oseltamivir is equal to the metabolic clearance of oseltamivir in the brain (*top right*), the efflux clearance of oseltamivir is much lower than the metabolic clearance of oseltamivir in the brain (*bottom left*), and the brain uptake of Ro 64-0802 is much larger than the brain metabolism (*bottom right*)

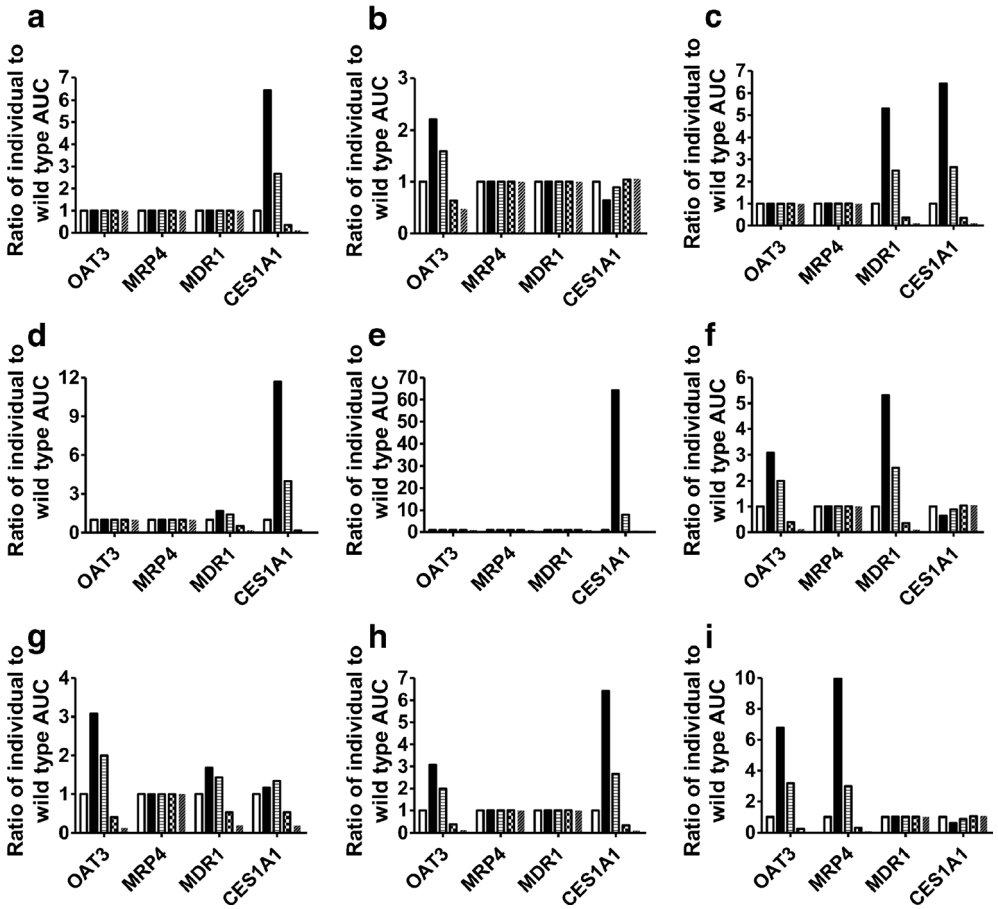

Fig. 7. Sensitivity analysis of the functional changes in each molecule. Each *column* represents the predictions when the functions of OAT3, MRP4, MDR1, and CES1A1 are (from *left* to *right*) intact (100%), decreased to 10% and 33%, and increased to 300% and 1000% compared with the wild type. The *vertical axis* represents the relative AUC ratio for each prediction normalized by the AUC obtained under the condition of intact function for all molecules (100%). The figures resrepresent blood AUC of a oseltamivir, b Ro 64-0802 and brain AUCs in the extreme cases of c efflux >> metabolism, d efflux = metabolism, e efflux << metabolism for oseltamivir, f efflux >> metabolism, g efflux = metabolism, h efflux << metabolism for oseltamivir in the brain under the condition of synthesis >> uptake for Ro 64-0802 in the brain, and i synthesis << brain uptake for Ro 64-0802 in the brain

CES1A1 contribute both systemically and centrally, the brain AUCs of oseltamivir are synergistically affected by CES1A1 function. By contrast, the AUC of Ro 64-0802 in the brain was affected predominantly by OAT3 in all scenarios (Fig. 7f–i) and by MRP4 when the brain uptake of Ro 64-0802 is greater than the rate of Ro 64-0802 synthesis in the brain (Fig. 7i). When the brain uptake of Ro 64-0802 is negligible compared with the rate of Ro 64-0802 synthesis in the brain, the AUC of Ro 64-0802 in the brain will be significantly affected by CES1A1 (Fig. 7h) and MDR1 (Fig. 7f), depending on the predominance of each metabolite there and efflux clearance of oseltamivir from the brain. Furthermore, we note that, even for the brain AUC for Ro 64-0802, reduced but not increased CES1A1 function caused an increase in the brain AUC for Ro 64-0802. This was seen in a scenario where brain metabolism of oseltamivir cannot be ruled out, which can be accounted for by synergistically increased brain AUCs for oseltamivir.

Sensitivity analysis showed clearly the importance of CES1A1 in AUC_{brain} of oseltamivir (Fig. 7c–e) and AUC_{brain} of Ro 64-0802 in a certain scenario (Fig. 7h). These data suggest that the hydrolysis activity of oseltamivir in the human brain should be examined. The lack of key information can be a critical constraint when performing this type of simulation. However, the use of a mathematical model allowed us to conduct uncertainty/sensitivity analysis to identify the effects of uncertainties, some of which are unknowns. This is one of the key aspects of the model-based approach.

Tarkiainen *et al.* investigated the effects of the CES1A1 SNP Gly143Glu (rs121912777), which reduced the catalytic efficiency by more than 80% (V_{max}/K_m) of CES1A1 for *p*-nitrophenyl acetate *in vitro* (40). In healthy Caucasian Finnish volunteers, the AUC_{inf} values in one homozygous carrier were ~290% and ~360% larger for oseltamivir and 20% and 27% smaller for Ro 64-0802 than the mean values in heterozygous carriers and noncarriers, respectively (41). Our predictions are in agreement with these findings. According to our simulation, the oseltamivir level in the brain will be markedly higher in a homozygous carrier than in a noncarrier.

We note the following limitations in the present study. First, we applied the mouse BBB characteristics to predict

human brain exposure under normal conditions. We also assumed that MRP4-mediated brain efflux of Ro 64-0802 is greater than the passive clearance. Therefore, the impact of functional changes in MRP4 directly influenced the brain influx clearance of Ro 64-0802, but not the efflux clearance because of uptake at the abluminal membrane being a rate-determining process in the overall efflux across the BBB under such condition. This assumption might also exaggerate the impact of functional changes in MRP4 on brain AUC of Ro 64-0802, as seen in Fig. 7i. Second, the effects of genetic mutations on the function of MDR1 are particularly controversial. Third, the CES1A1-mediated hydrolysis of oseltamivir has not been elucidated, but was assumed to be much higher than that of nonenzymatic hydrolysis in the human brain. Finally, although age and body weight have been shown to be significant covariates for total clearance of Ro 64-0802 (application form), because of a lack of more detailed information, pharmacokinetic parameters used in this study were obtained based on data from adults. One must be prudent when interpreting the simulation outcomes because of the uncertainties within these assumptions. On the other hand, when performing this sort of model-based risk assessment, some assumptions are necessary because not all of the information is available. We believe it is more effective to build mathematical models and run simulations under several assumptions with uncertainties and to identify the key components and molecules that play pivotal roles. This practice improves the efficiency and effectiveness of drug research and development (and even applications in postmarketing surveillance) because it always provides quantitative answers to fundamental questions and insights into the worst-case scenario based on current knowledge and helps to prioritize the uncertainties and assumptions that should be solved.

Concerning the effects of genetic mutation on MDR1, a positron emission tomography study using ^{11}C-verapamil found no significant differences between three haplotypes of the MDR1 gene: SNPs C1236T, G2677T, and C3435T (42). However, substrate specificity might exist. In support of this hypothesis, Kimchi-Sarfaty *et al.* reported that the affinities of MDR1 against cyclosporine A, verapamil, and rapamycin differed between some variants despite the lack of differences in amino acid sequences (43).

Finally, although the clinical relevance of these findings needs further investigation and should be interpreted carefully, the risk assessment approach using Monte Carlo simulation and including interindividual variability may be useful in understanding unexpected drug exposure that could cause rare, but unacceptable, future events. More importantly, the model-based approach offers an iterative "learn and confirm" cycle including insightful information such as what is known and unknown, the magnitude of uncertainty, and whether and how to proceed to the next step.

CONCLUSION

The Monte Carlo simulation analyses showed the systemic AUC of oseltamivir and Ro 64-0802 were increased by at most threefold, whereas the brain AUCs were increased up to about sevenfold (oseltamivir) and 40-fold (Ro 64-0802), compared with the population means. The risk assessment approach by using Monte Carlo simulation taking interindividual variability (caused by inherent genetic mutations as well as random variability) into consideration is useful to better understand the unexpected drug exposure which could cause unacceptable events that might happen with rare frequency.

AUC, area under the curve; BBB, blood–brain barrier; CES, carboxylesterase; CNS, central nervous system; CSF, cerebrospinal fluid; CV, coefficient of variations; E_h, extraction in the liver; EC_{50}, half maximal effective concentration; E-sul, estron-3-sulfate; F_a, fraction of absorbed; F_g, availability in the intestine; HEK, human embryonic kidney; MDR, multidrug resistance; MRP, multidrug resistance-associated protein; NPAEs, neuropsychiatric adverse events; OAT, organic anion transporter; OCT; organic cation transporter; PAH, *p*-aminohippurate; P-gp, P-glycoprotein; PS, permeability surface area product; TEA, tetraethylammonium

ACKNOWLEDGMENTS

We thank Dr. Kenzo Yamatsugu, Dr. Motomu Kanai, and Dr. Masakatsu Shibasaki for providing oseltamivir and Ro 64-0802. We also thank Dr. Junko Iida and Futoshi Kurotobi (Shimadzu Corporation, Kyoto, Japan) for the technical support of the LC/MS system.

This study was financially supported by Grant-in-Aid for Scientific Research (S) and (B) [Grant 24229002 and 26293032].

REFERENCES

1. Toovey S, Prinssen EP, Rayner CR, Thakrar BT, Dutkowski R, Koerner A, *et al*. Post-marketing assessment of neuropsychiatric adverse events in influenza patients treated with oseltamivir: an updated review. Adv Ther. 2012;29(10):826–48.
2. Toovey S, Rayner C, Prinssen E, Chu T, Donner B, Thakrar B, *et al*. Assessment of neuropsychiatric adverse events in influenza patients treated with oseltamivir: a comprehensive review. Drug Saf. 2008;31(12):1097–114.
3. Yoshino T, Nisijima K, Shioda K, Yui K, Kato S. Oseltamivir (Tamiflu) increases dopamine levels in the rat medial prefrontal cortex. Neurosci Lett. 2008;438(1):67–9.
4. Ono H, Nagano Y, Matsunami N, Sugiyama S, Yamamoto S, Tanabe M. Oseltamivir, an anti-influenza virus drug, produces hypothermia in mice. Biol Pharm Bull. 2008;31(4):638–42.
5. Suzuki M, Masuda Y. Effect of a neuraminidase inhibitor (oseltamivir) on mouse jump-down behavior via stimulation of dopamine receptors. Biomed Res. 2008;29(5):233–8.
6. Izumi Y, Tokuda K, O'Dell KA, Zorumski CF, Narahashi T. Neuroexcitatory actions of Tamiflu and its carboxylate metabolite. Neurosci Lett. 2007;426(1):54–8.
7. Usami A, Sasaki T, Satoh N, Akiba T, Yokoshima S, Fukuyama T, *et al*. Oseltamivir enhances hippocampal network synchronization. J Pharmacol Sci. 2008;106(4):659–62.
8. Takashima T, Yokoyama C, Mizuma H, Yamanaka H, Wada Y, Onoe K, *et al*. Developmental changes in P-glycoprotein function

in the blood–brain barrier of nonhuman primates: PET study with R-11C-verapamil and 11C-oseltamivir. J Nucl Med. 2011;52(6):950–7.
9. Seki C, Oh-Nishi A, Nagai Y, Minamimoto T, Obayashi S, Higuchi M, *et al.* Evaluation of [(11)C]oseltamivir uptake into the brain during immune activation by systemic polyinosine-polycytidylic acid injection: a quantitative PET study using juvenile monkey models of viral infection. EJNMMI Res. 2014;4:24.
10. Ose A, Ito M, Kusuhara H, Yamatsugu K, Kanai M, Shibasaki M, et al. Limited brain distribution of Ro 64-0802, a pharmacologically active form of oseltamivir, by active efflux across the blood-brain barrier mediated by organic anion transporter 3 (Oat3/Slc22a8) and multidrug resistance-associated protein 4 (Mrp4/Abcc4). Drug Metab Dispos. 2008.
11. Ose A, Kusuhara H, Yamatsugu K, Kanai M, Shibasaki M, Fujita T, *et al.* P-glycoprotein restricts the penetration of oseltamivir across the blood–brain barrier. Drug Metab Dispos. 2008;36(2):427–34.
12. Shi D, Yang J, Yang D, LeCluyse EL, Black C, You L, *et al.* Anti-influenza prodrug oseltamivir is activated by carboxylesterase human carboxylesterase 1, and the activation is inhibited by antiplatelet agent clopidogrel. J Pharmacol Exp Ther. 2006;319(3):1477–84.
13. Yamatsugu K, Yin L, Kamijo S, Kimura Y, Kanai M, Shibasaki M. A synthesis of Tamiflu by using a barium-catalyzed asymmetric Diels-Alder-type reaction. Angew Chem Int Ed Engl. 2009;48(6):1070–6.
14. Nozaki Y, Kusuhara H, Kondo T, Hasegawa M, Shiroyanagi Y, Nakazawa H, *et al.* Characterization of the uptake of organic anion transporter (OAT) 1 and OAT3 substrates by human kidney slices. J Pharmacol Exp Ther. 2007;321(1):362–9.
15. Deguchi T, Kusuhara H, Takadate A, Endou H, Otagiri M, Sugiyama Y. Characterization of uremic toxin transport by organic anion transporters in the kidney. Kidney Int. 2004;65(1):162–74.
16. Nishizato Y, Ieiri I, Suzuki H, Kimura M, Kawabata K, Hirota T, *et al.* Polymorphisms of OATP-C (SLC21A6) and OAT3 (SLC22A8) genes: consequences for pravastatin pharmacokinetics. Clin Pharmacol Ther. 2003;73(6):554–65.
17. Hirano M, Maeda K, Shitara Y, Sugiyama Y. Contribution of OATP2 (OATP1B1) and OATP8 (OATP1B3) to the hepatic uptake of pitavastatin in humans. J Pharmacol Exp Ther. 2004;311(1):139–46.
18. Iwai M, Suzuki H, Ieiri I, Otsubo K, Sugiyama Y. Functional analysis of single nucleotide polymorphisms of hepatic organic anion transporter OATP1B1 (OATP-C). Pharmacogenetics. 2004;14(11):749–57.
19. Lindegardh N, Davies GR, Tran TH, Farrar J, Singhasivanon P, Day NP, *et al.* Rapid degradation of oseltamivir phosphate in clinical samples by plasma esterases. Antimicrob Agents Chemother. 2006;50(9):3197–9.
20. Wiltshire H, Wiltshire B, Citron A, Clarke T, Serpe C, Gray D, *et al.* Development of a high-performance liquid chromatographic-mass spectrometric assay for the specific and sensitive quantification of Ro 64-0802, an anti-influenza drug, and its pro-drug, oseltamivir, in human and animal plasma and urine. J Chromatogr B Biomed Sci Appl. 2000;745(2):373–88.
21. He G, Massarella J, Ward P. Clinical pharmacokinetics of the prodrug oseltamivir and its active metabolite Ro 64-0802. Clin Pharmacokinet. 1999;37(6):471–84.
22. Wynne HA, Cope LH, Mutch E, Rawlins MD, Woodhouse KW, James OF. The effect of age upon liver volume and apparent liver blood flow in healthy man. Hepatology. 1989;9(2):297–301.
23. Razzak MA, Botti RE, MacIntyre WJ. Interrelationship between hydration, urine flow, renal blood flow and the radiohippuran renogram. J Nucl Med. 1969;10(11):672–5.
24. Kato M, Chiba K, Ito T, Koue T, Sugiyama Y. Prediction of interindividual variability in pharmacokinetics for CYP3A4 substrates in humans. Drug Metab Pharmacokinet. 2010;25(4):367–78.
25. Davies B, Morris T. Physiological parameters in laboratory animals and humans. Pharm Res. 1993;10(7):1093–5.
26. Kato M, Tachibana T, Ito K, Sugiyama Y. Evaluation of methods for predicting drug-drug interactions by Monte Carlo simulation. Drug Metab Pharmacokinet. 2003;18(2):121–7.
27. Erdman AR, Mangravite LM, Urban TJ, Lagpacan LL, Castro RA, de la Cruz M, *et al.* The human organic anion transporter 3 (OAT3; SLC22A8): genetic variation and functional genomics. Am J Physiol Renal Physiol. 2006;290(4):F905–12.
28. Xu G, Bhatnagar V, Wen G, Hamilton BA, Eraly SA, Nigam SK. Analyses of coding region polymorphisms in apical and basolateral human organic anion transporter (OAT) genes [OAT1 (NKT), OAT2, OAT3, OAT4, URAT (RST)]. Kidney Int. 2005;68(4):1491–9.
29. Geshi E, Kimura T, Yoshimura M, Suzuki H, Koba S, Sakai T, *et al.* A single nucleotide polymorphism in the carboxylesterase gene is associated with the responsiveness to imidapril medication and the promoter activity. Hypertens Res. 2005;28(9):719–25.
30. Krishnamurthy P, Schwab M, Takenaka K, Nachagari D, Morgan J, Leslie M, *et al.* Transporter-mediated protection against thiopurine-induced hematopoietic toxicity. Cancer Res. 2008;68(13):4983–9.
31. Salama NN, Yang Z, Bui T, Ho RJ. MDR1 haplotypes significantly minimize intracellular uptake and transcellular P-gp substrate transport in recombinant LLC-PK1 cells. J Pharm Sci. 2006;95(10):2293–308.
32. Morita N, Yasumori T, Nakayama K. Human MDR1 polymorphism: G2677T/A and C3435T have no effect on MDR1 transport activities. Biochem Pharmacol. 2003;65(11):1843–52.
33. Hung CC, Chiou MH, Teng YN, Hsieh YW, Huang CL, Lane HY. Functional impact of ABCB1 variants on interactions between P-glycoprotein and methadone. PLoS ONE. 2013;8(3):e59419.
34. Kato M, Fukuda T, Serretti A, Wakeno M, Okugawa G, Ikenaga Y, *et al.* ABCB1 (MDR1) gene polymorphisms are associated with the clinical response to paroxetine in patients with major depressive disorder. Prog Neuropsychopharmacol Biol Psychiatry. 2008;32(2):398–404.
35. Yamada T, Hosokawa M, Satoh T, Moroo I, Takahashi M, Akatsu H, *et al.* Immunohistochemistry with an antibody to human liver carboxylesterase in human brain tissues. Brain Res. 1994;658(1–2):163–7.
36. Hill G, Cihlar T, Oo C, Ho ES, Prior K, Wiltshire H, *et al.* The anti-influenza drug oseltamivir exhibits low potential to induce pharmacokinetic drug interactions via renal secretion-correlation of in vivo and in vitro studies. Drug Metab Dispos. 2002;30(1):13–9.
37. Watanabe T, Kusuhara H, Watanabe T, Debori Y, Maeda K, Kondo T, *et al.* Prediction of the overall renal tubular secretion and hepatic clearance of anionic drugs and a renal drug-drug interaction involving organic anion transporter 3 in humans by in vitro uptake experiments. Drug Metab Dispos. 2011;39(6):1031–8.
38. van Crugten J, Bochner F, Keal J, Somogyi A. Selectivity of the cimetidine-induced alterations in the renal handling of organic substrates in humans. Studies with anionic, cationic and zwitterionic drugs. J Pharmacol Exp Ther. 1986;236(2):481–7.
39. Jhee SS, Yen M, Ereshefsky L, Leibowitz M, Schulte M, Kaeser B, *et al.* Low penetration of oseltamivir and its carboxylate into cerebrospinal fluid in healthy Japanese and Caucasian volunteers. Antimicrob Agents Chemother. 2008;52(10):3687–93.
40. Zhu HJ, Patrick KS, Yuan HJ, Wang JS, Donovan JL, DeVane CL, *et al.* Two CES1 gene mutations lead to dysfunctional carboxylesterase 1 activity in man: clinical significance and molecular basis. Am J Hum Genet. 2008;82(6):1241–8.
41. Tarkiainen EK, Backman JT, Neuvonen M, Neuvonen PJ, Schwab M, Niemi M. Carboxylesterase 1 polymorphism impairs oseltamivir bioactivation in humans. Clin Pharmacol Ther. 2012;92(1):68–71.
42. Takano A, Kusuhara H, Suhara T, Ieiri I, Morimoto T, Lee YJ, *et al.* Evaluation of in vivo P-glycoprotein function at the blood–brain barrier among MDR1 gene polymorphisms by using 11C-verapamil. J Nucl Med. 2006;47(9):1427–33.
43. Kimchi-Sarfaty C, Oh JM, Kim IW, Sauna ZE, Calcagno AM, Ambudkar SV, *et al.* A "silent" polymorphism in the MDR1 gene changes substrate specificity. Science. 2007;315(5811):525–8.